

# Scene Categorization with Spectral Features

Salman H. Khan<sup>1,3</sup>, Munawar Hayat<sup>2</sup> and Fatih Porikli<sup>3</sup>

<sup>1</sup>Data61-CSIRO, <sup>2</sup>University of Canberra, <sup>3</sup>Australian National University

{salman.khan, fatih.porikli}@anu.edu.au, munawar.hayat@canberra.edu.au

## Abstract

*Spectral signatures of natural scenes were earlier found to be distinctive for different scene types with varying spatial envelope properties such as openness, naturalness, ruggedness, and symmetry. Recently, such handcrafted features have been outclassed by deep learning based representations.*

*This paper proposes a novel spectral description of convolution features, implemented efficiently as a unitary transformation within deep network architectures. To the best of our knowledge, this is the first attempt to use deep learning based spectral features explicitly for image classification task. We show that the spectral transformation decorrelates convolutional activations, which reduces co-adaptation between feature detections, thus acts as an effective regularizer. Our approach achieves significant improvements on three large-scale scene-centric datasets (MIT-67, SUN-397, and Places-205). Furthermore, we evaluated the proposed approach on the attribute detection task where its superior performance manifests its relevance to semantically meaningful characteristics of natural scenes.*

## 1. Introduction

Scene recognition is a challenging task with a broad range of applications in content-based image indexing and retrieval systems. The knowledge about the scene category can also assist in context-aware object detection, action recognition, and scene understanding [29, 64]. Spectral signature of an image has been shown to be distinctive and semantically meaningful for indoor and outdoor scenes. Initial work from Oliva *et al.* [37] used power spectrum as a global feature descriptor to characterize scenes. Later, Torralba and Oliva proposed a spatial envelope model that estimates the shape of a scene (a.k.a. ‘the gist’) using the statistics of both global and localized spectral information [36, 54]. However, these global features work only for categorization of scenes into a general set of classes (e.g., beach, highway, forest, and mountain) and fail to tackle fine-grained scene classification, which involves discriminating highly confusing scene categories with subtle differences (e.g., bus station, train station, and airport).

In this work, we propose to use spectral features obtained from intermediate convolutional layer activations of

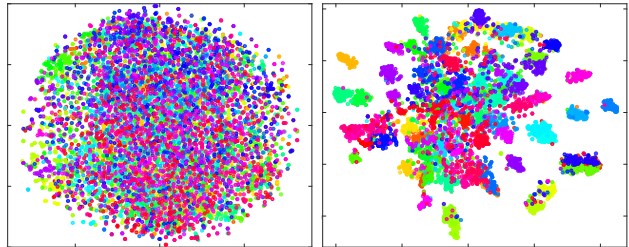


Figure 1: t-SNE visualization of gist and spectral features for the MIT-67 indoor scene dataset. (Best viewed in color)

deep neural networks for scene classification (Fig. 1). We demonstrate that these feature representations perform surprisingly well for the scene categorization task and result in significant performance gains. Further, these spectral features can be used to automatically tag scenes with semantically meaningful attributes (e.g., man-made, dense, natural). These attributes not only pertain to appearance based characteristics but also relate to functional and material properties, illustrating that the learned spectral features can capture meaningful information about a scene, closely linked with the mid-level, human-interpretable attributes. Such a global scene-centric representation can be computed efficiently without involving segmentation, detection, and grouping procedures. Therefore, it could assist in local image analysis or as an attention mechanism to focus on specific details in complex and cluttered scenes. It is noteworthy to point out that such a visual processing approach is consistent with the remarkable ability of human visual perception which quickly identifies a scene in its first glance and uses this information to selectively attend to the salient scene details at a finer scale [5, 55].

The proposed spectral features are derived from the learned convolutional activations in a deep neural network using an orthogonal unitary transformation. Orthogonal transforms possess decorrelation properties, thus they tend to concentrate feature energy into only a small number of coefficients [2]. In terms of decorrelation and energy compaction, Karhunen-Loeve Transform (KLT) provides an optimal solution [1] by identifying the principle directions (eigenvectors) of the data covariance matrix and projecting the data onto these orthogonal basis to achieve maximal decorrelation (independence) and energy compaction (concentration). However, a serious drawback of KLT is its high

computational cost ( $\mathcal{O}(n^2)$  complexity), which prevents its deployment to large-scale scene classification problems.

We show that for a large number of neurons, KLT can be well approximated by the spectral-domain discrete Fourier transforms. These approximations can be efficiently computed, thanks to the fast algorithms that utilize precomputed basis functions. A beneficial consequence of a spectral transformation is that it tends to regularize the deep network by reducing feature co-adaptations and therefore enhances its generalization ability. Previous literature demonstrates the significance of having uncorrelated and disentangled representations for supervised and unsupervised learning tasks [8, 52, 12]. Another major motivation is that the human visual sensory mechanism also favors sparse and non-redundant representations [57].

Deep neural networks with fixed parameters, such as the wavelet scattering networks [9, 26, 49], have been reported to perform efficiently for specific tasks. However, these rigid architectures do not generalize and are outperformed by data-driven features. As an alternative, we propose a spectral transformation of Convolutional Neural Network (CNN) activations on fixed basis vectors while learning the rest of the network parameters from data. We demonstrate that the spectral transformation with fixed parameters achieves better classification performance than the conventionally learned parameters. The resulting architecture not only performs superior on task-specific learning problems but also generalizes to transfer learning scenarios.

We report performance improvements on three large-scale scene classification datasets, MIT-67, SUN-397 and Places-205. Furthermore, our experiments on two attribute datasets (SUN Attribute and Outdoor Scene Attribute) show significant performance gains. In addition to the improved classification performance, the spectral transformation does not require any additional supervision or data dependent statistics to enforce independence between feature detectors. Its integration within any CNN architecture is straightforward, and a unitary transformation could be achieved with insignificant additional computation load during the training and testing processes.

We review related approaches in § 2. Our proposed feature representation is described in § 3 and the experiments on scene classification and attribute recognition are summarized in § 4 and § 5, respectively. A comprehensive ablation analysis is provided in § 4.4 as well.

## 2. Related Work

**Scene Classification:** Popular approaches reported in the literature for scene classification use global descriptors [62, 36], mid-level distinctive parts [27, 15], bag-of-word style models [33, 6], and deep neural networks [29, 46]. Recent best performing methods on scene recognition either employ feature encoding approaches on CNN activations

[17, 22] or leverage from large-scale scene-centric datasets [67] and feature jittering [20]. In contrast to these works, we introduce a simple and efficient solution to obtain high-performing spectral features within regular CNNs, which is computationally inexpensive (in comparison to feature encoding methods), efficiently generalizable, and able to benefit from large-scale scene datasets.

**Deep Networks:** CNNs have obtained state-of-the-art performance on several key computer vision tasks including classification [31, 21], detection [47, 30], localization [66], segmentation [34], and retrieval [3]. Beginning with the rudimentary LeNet model, several revamped and extended architectures (e.g., AlexNet [31], GoogLeNet [53], VGGnet [51], and ResNet [23]) have been proposed for image classification. More specialized models such as FCN [34] and R-CNN [47] have been used for segmentation and localization. All of these models have been learned in a data-driven manner from the raw data. In contrast, our work proposes a simple spectral transformation layer that provides significant improvements, although its parameters do not require learning. Previous works that use fixed or random parameter layers had limited generalization properties and suffered from performance degradation [26, 40, 49].

**Spectral Representations:** According to the convolution theorem, there exists an equivalence between convolution operation in the spatial domain and point-wise multiplication in the spectral domain [38]. Therefore, frequency domain transforms have traditionally been considered in deep networks to achieve computational gains [4, 35]. For small convolution kernels (e.g.,  $3 \times 3$  in state-of-the-art VGGnet model) computational gain was found to be minimal [56, 32]. Similarly, spectral transforms along with hashing techniques have been used to reduce the memory footprint of the deep networks by eliminating redundancy [10, 11]. In this work, we show that spectral features are more powerful for classification than their counterparts in the spatial domain. In this aspect, our work is relevant to the spectral pooling [48] approach that improves the down sampling process by retaining informative frequency coefficients.

**Regularization:** Feature co-adaptations are avoided in [52, 58] by randomly reducing neurons or their connections to zero during the training process. Batch normalization is another popular approach that indirectly improves generalization capacity by minimizing the internal covariance shifts [25]. There is also recent work on imposing sparsity in network layers [68] and using modified losses to avoid imbalanced set representations [28]. These methods, however, do not explicitly decorrelate individual feature detectors. Some recent approaches [14, 12] employ covariance based loss functions as regularizers to reduce co-adaptations during the training process. Different from these works, our approach uses a spectral transformation to decorrelate feature detectors without any explicit training regime.

### 3. Proposed Approach

KLT is one of the ideal choices in terms of signal decorrelation, data compression, and energy compaction. Given a symmetric positive semi-definite data covariance matrix,  $C_n \in \mathbb{R}^{n \times n}$ , the KLT basis vectors ( $\Phi_i$ ) can be obtained by solving the following eigenvalue problem:

$$(C_n - \lambda_i \mathcal{I}_n) \Phi_i = 0, \quad i \in [1, n] \quad (1)$$

where,  $\lambda_i$  are the eigenvalues and  $\mathcal{I}$  represents identity matrix. It is evident from Eq. 1 that the basis functions for KLT can not be predetermined due to their dependence on the data covariance matrix. Therefore, the diagonalization of covariance matrix to generate KLT basis vectors is a computationally expensive process (especially when  $n$  is large).

For high dimensional data, the Discrete Fourier Transform (DFT) of the covariance matrix of a stationary first-order Markov signal is asymptotically equivalent to its KLT [18]. Note that for a first-order Markov process, the data covariance matrix has a symmetric Toeplitz structure which is asymptotically equivalent to a circulant matrix for a large  $n$  (it is well known that the eigenvectors of a circulant matrix are the basis of DFT). Here, we first show that spectral transformation of convolutional activations has a decorrelation effect. Note that the following analysis has particular relevance to CNN activations which have high dimensionality and somewhat low correlation beforehand.

Suppose that  $C_n$  denotes the class of covariance matrices which model the correlation between  $n$  feature detectors in a fully-connected layer ( $\ell$ ) of the CNN:

$$C_n = \text{cov}(F) = \mathbb{E}[(F - \mathbb{E}(F))(F - \mathbb{E}(F))^T],$$

where,  $F \in \mathbb{R}^{n \times m}$  is the matrix comprising of  $n$ -dimensional feature vectors corresponding to  $m$  images. Since the convolutional activations are real valued,  $C_n$  represents real symmetric matrices i.e.,  $C_n = C_n^T$  and  $\text{Im}(C_n) = \mathbf{0}^{n \times n}$ . The feature detectors generate  $m$  responses corresponding to a given dataset  $\mathcal{X} = \{X_1, \dots, X_m\}$ . Also, consider  $\mathcal{T}_n \in \mathbb{R}^{n \times n}$  to be a class of Toeplitz (constant-diagonal) matrices whose elements are defined as,  $\mathcal{T}_n^{i,j} = \tau_{i-j}$ , where  $\tau_{i-j}$  is a constant from the set  $\{\tau_{1-n}, \dots, \tau_{n-1}\}$ . In the following theorem, we establish equivalence between the two classes of matrices,  $C_n$  and  $\mathcal{T}_n$ , under certain conditions.

**Theorem 3.1.** *For a large number of feature detectors  $n$  in layer  $\ell$ , the process is asymptotically weakly stationary such that:  $C_n \sim \mathcal{T}_n$ , where  $\sim$  denotes asymptotic equivalence.*

*Proof.* Asymptotic equivalence between  $C_n$  and  $\mathcal{T}_n$  can be proved by satisfying the following two properties [45]:

- The matrix classes  $C_n$  and  $\mathcal{T}_n$  are bounded in terms of both operator and Hilbert-Schmidt norms (lemma 3.2).

<sup>1</sup> $\text{Im}(\cdot)$  denotes the imaginary part.

- The Hilbert-Schmidt norm of the matrix difference  $(C_n - \mathcal{T}_n)$  vanishes when  $n$  is large (lemma 3.3).

We prove these properties below.  $\square$

**Lemma 3.2.** *The matrix classes  $C_n$  and  $\mathcal{T}_n$  are strongly bounded such that:*

$$\|C_n\|, \|\mathcal{T}_n\| < z < \infty \quad (2)$$

*Proof.* Here, we only consider the matrix class  $C_n$  and note that similar arguments can be applied for matrix class  $\mathcal{T}_n$ . Since,  $C_n$  is Hermitian, its operator norm is defined as:

$$\|C_n\| = \sup_{\mathbf{y} \in \mathbb{R}^n: \langle \mathbf{y}, \mathbf{y} \rangle = 1} \mathbf{y}^T C_n \mathbf{y} = \max_i |\lambda_C^i|.$$

We assume that the individual entries of the covariance matrix  $C_n$  are bounded:  $|C_n^{i,j}| \leq u$ . Furthermore, the off-diagonal entries are smaller compared to the diagonal:

$$\left| \frac{C_n^{i,j}}{C_n^{i,i}} \right| \leq 1 \quad : j \neq i.$$

Using the Gershgorin circle theorem, we can see that the eigenvalues of  $C_n$  are bounded by the Gershgorin discs,

$$s.t., \quad \max_i |\lambda_C^i| < D(C_n^{i,i}, \sum_{j \neq i} |C_n^{i,j}|).$$

A matrix bounded in the operator norm is also bounded in the Hilbert-Schmidt norm, since:  $|C_n| \leq \|C_n\|$ . Hence, Eq. 2 is the necessary and sufficient condition to satisfy the first property.  $\square$

**Lemma 3.3.** *The Hilbert-Schmidt norm of the matrix difference between  $C_n$  and  $\mathcal{T}_n$  vanishes as  $n \rightarrow \infty$ , i.e.,*

$$\lim_{n \rightarrow \infty} |C_n - \mathcal{T}_n| = 0. \quad (3)$$

*Proof.* Since both  $C_n$  and  $\mathcal{T}_n$  are Hermitian, we can decompose them as follows:

$$C_n = P_n \Sigma_C P_n^T, \quad \mathcal{T}_n = Q_n \Sigma_{\mathcal{T}} Q_n^T.$$

Here,  $P_n, Q_n$  are the unitary transforms which diagonalize the covariance matrices  $C_n$  and  $\mathcal{T}_n$  to:

$$\Sigma_C = \text{diag}(\lambda_C^i), \quad \Sigma_{\mathcal{T}} = \text{diag}(\lambda_{\mathcal{T}}^i),$$

where,  $\lambda_C^i$  and  $\lambda_{\mathcal{T}}^i$  denote the eigen values,  $i \in [1, n]$ . Consider the matrix class  $C_n$  under the unitary transformation  $Q_n$  to be:

$$A_n = Q_n^T C_n Q_n = Q_n^T P_n \Sigma_C P_n^T Q_n. \quad (4)$$

Approximating  $A_n$  as:  $\tilde{A}_n = \text{diag}(A_n)$ , the projection onto  $P_n$  can be defined as:  $\psi_Q[C_n] = P_n \tilde{A}_n P_n^T$ . The asymptotic equivalence can then be established considering the Hilbert-Schmidt norm of the difference between  $C_n$  and its projec-

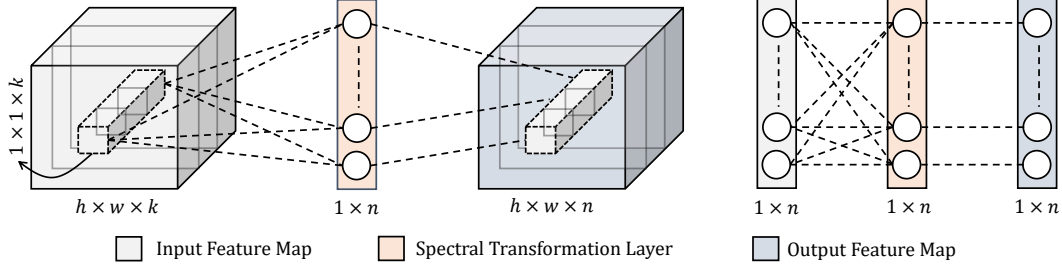


Figure 2: As shown, the spectral transformation is implemented as a convolutional layer in the CNN model. The transformation can be used after a fully-connected layer (*right*) as a convolutional layer (*left*) as well.

tion  $\psi_Q[C_n]$ :

$$|C_n - \psi_Q[C_n]| = \sqrt{\frac{1}{n} \sum_{i=1}^n (\lambda_C^i{}^2 - \tilde{A}_n^{i,i}{}^2)}. \quad (5)$$

Here,  $\lambda_C^i{}^2$  and  $\tilde{A}_n^{i,i}{}^2$  can be represented in terms of matrix product as follows:

$$\sum_{i=1}^n \lambda_C^i{}^2 = \lambda_C \lambda_C^T, \quad \sum_{i=1}^n \tilde{A}_n^{i,i}{}^2 = \tilde{A}_n \tilde{A}_n^T = \lambda_C B_n B_n^T \lambda_C^T$$

where,  $\lambda_C$  is the vector of all eigenvalues of  $C_n$  and  $B_n = \text{diag}(Q_n^T P_n) = \text{diag}(\langle \mathbf{q}_k, \mathbf{p}_k \rangle)$  s.t.  $k \in [1, n]$ , where  $\mathbf{q}_k, \mathbf{p}_k$  are the columns of matrices  $Q_n, P_n$  respectively. Substituting the above expressions in Eq.5:

$$|C_n - \psi_Q[C_n]| = \sqrt{\frac{1}{n} (\lambda_C (I_n - B_n B_n^T) \lambda_C^T)}. \quad (6)$$

Here, the eigenvalues are bounded (as per lemma 3.2). Furthermore, since the matrices  $Q_n, P_n$  are unitary, the sum  $\sum_{i=1}^n (\tilde{A}_n^{i,i})^2$  is also bounded and therefore:

$$\lim_{n \rightarrow \infty} |C_n - \psi_Q[C_n]| = 0,$$

which proves the lemma.  $\square$

Having the asymptotic equivalence established, we quote two important results [7, 19]. The corollary 3.3.1 immediately follows from the lemma 3.3 and the Wielandt-Hoffman theorem [24] for Hermitian matrices, while the corollary 3.3.2 follows from the lemma 3.2 [18].

**Corollary 3.3.1.** *If matrix classes  $C_n$  and  $T_n$  with eigenvalues  $\lambda_C^i$  and  $\lambda_T^i$  are asymptotically equivalent, we have:*

$$\lim_{n \rightarrow \infty} \frac{1}{n} \sum_{i=1}^n (\lambda_C^i - \lambda_T^i) = 0$$

**Corollary 3.3.2.** *If two matrix classes  $C_n$  and  $T_n$  with eigen-values  $\lambda_C^i$  and  $\lambda_T^i$  are asymptotically equivalent such that  $\lambda_C^i, \lambda_T^i$  have a lower bound  $z' > 0$ , then:*

$$\lim_{n \rightarrow \infty} \sqrt[n]{\det C_n} - \sqrt[n]{\det T_n} = 0$$

Next, we describe the details of the spectral transformation used in our CNN model.

### 3.1. Spectral Transform

Having established the asymptotic equivalence between the KLT and the DFT for a general class of discrete signals, we investigate efficient ways to implement spectral transformation within a deep neural network. Although, fast algorithms for DFT computation are available (e.g., Fast Fourier Transform), a complex Fourier transform seems less desirable because phase information is not much useful for classification. Furthermore, our experiments show that a closely related real-valued DCT transform performs slightly better in practice (see § 4.4 for details). The spectral transform is implemented as a convolution layer which can be placed at any level in the CNN architecture. Given an input activations tensor  $Y_{\ell-1}$  from the  $\ell - 1$  layer, we have:

$$Y_{\ell}^s = Y_{\ell-1}^t * k_{\ell}^{t,s}, \quad (7)$$

where ‘\*’ denotes the convolution operation and  $k$  denotes  $1 \times 1$  dimensional filter which maps the  $t^{th}$  feature map from the input tensor to the  $s^{th}$  feature map of the output tensor. An illustration of the spectral transformation layer implementation in a CNN is given in Fig. 2.

### 3.2. Complexity Analysis

Computational complexity of a convolution operation per kernel is  $\mathcal{O}(n^2 k^2)$  for an  $n \times n$  input and a  $k \times k$  kernel (normally  $n \gg k$ ). Previous works apply Fast Fourier Transform (FFT) for spectral transformation which leads to efficient computations due to equivalent Hadamard products in the spectral domain [35, 38]. However, the FFT computation introduces an additional transformation cost of  $\mathcal{O}(n^2 \log_2 n^2)$ . In comparison, our approach only requires a matrix multiplication in the Fully-Connected (FC) layers and a  $1 \times 1$  convolution operation in the intermediate convolution layers leading to a cost of  $\mathcal{O}(n^2)$  in both cases. We notice that a direct FFT transform has a lower computational cost of  $\mathcal{O}(n \log n)$ , however a standard convolutional layer based implementation allows the adaptation of preceding network layers via error propagation. Such an implementation is also efficient since it uses fast BLAS rou-



Figure 3: Qualitative results on the Places-205 dataset shows more informative regions in an image using a heat map.

Approach	Accuracy (%)
OOM-semClusters [16]	68.6
CNN-MOP [17]	68.9
CNNaug-SVM [50]	69.0
Hybrid-CNN [67]	70.8
SSICA-CNN [20]	74.4
Places-CNDS [60]	76.1
Deep Filter Banks [13]	81.0
Baseline CNN (Places-VGGnet [59])	80.9
Places VGGnet + Spectral Features	<b>84.3</b>

Table 1: Average accuracy on the MIT-67 Indoor Scene dataset. For fairness, we only report comparisons with methods based on deep networks.

times for matrix multiplication. Furthermore, since we are harnessing spectral representations, we do not require the transformation back to the spectral domain as in [35].

## 4. Scene Classification

### 4.1. Implementation Details

We used a VGGnet-16 model trained on the Places-205 dataset [59]. The VGGnet has demonstrated excellent performances on the object detection and scene classification tasks [51, 29]. The spectral transformation layer is deployed before the first FC layer, and the network is fine-tuned with relatively high learning rates in the subsequent FC layers but very small learning rates in the earlier convolution layers. An equidimensional spectral transformation has been applied; thus the input to the first FC layer still remains a 4096-dimensional feature vector. For training the network, we augment each image with its flipped, cropped, and rotated versions [20]. Specifically, from the original image, we first crop five images (four from the corners and one from the center). We then rotate the original image by  $\frac{\pi}{6}$  and  $-\frac{\pi}{6}$  radians. Finally, we horizontally flip all these eight images (one original, five cropped and two rotated). The augmented set of an image, therefore, has 16 images.

### 4.2. Datasets

**MIT-67 Dataset** [42] contains a total of 15,620 images belonging to 67 indoor scene classes. For our experiments, we follow the standard evaluation protocol, which uses a train and test split of 80% – 20% for each class.

**Places-205 Dataset** [67] is a large-scale scene-centric

Approach	Accuracy (%)
Places-AlexNet [67]	50.0
Places-GoogLeNet [53]	55.5
Places-CNDS [60]	55.7
Places-VGGnet-11 [59]	59.0
Baseline CNN (Places-VGGnet [59])	60.3
Places VGGnet + Spectral Features	<b>61.2</b>

Table 2: Average accuracy on the Places-205 Scene Dataset.

dataset containing nearly 2.5 million labeled images. Each scene category contains 5,000-15,000 images for training, 100 images for validation and 200 images for testing.

**SUN-397 Dataset** [64] consists of 108,754 images belonging to 397 categories. Each scene category contains at least 100 images. The dataset is divided into 10 train/test splits, each split comprising of 50 train images and 50 test images per category.

It is important to note that the Places and SUN datasets use several same scene categories based on the WordNet hierarchy, however both datasets do not contain any overlapping images, and therefore, have complementary strengths.

### 4.3. Results

Our experimental results on the MIT-67, Places-205 and SUN-397 datasets are presented in Table 1, 2 and 3 respectively. As a baseline, we use features extracted from VGGnet-16 pre-trained on the Places-205 dataset [59] and fine-tuned on the respective dataset. For comparison with existing methods, we only report performances of methods that employ learned feature representations from deep neural networks. The experimental results in Tables 1, 2 and 3 indicate the effectiveness of the proposed spectral features. Specifically, we noticed a consistent relative improvement of 4.2%, 1.5% and 1.0% on the MIT-67, Places-205 and SUN-397 datasets respectively. Class-wise improvements in classification accuracy for spectral features on MIT-67 dataset are shown in Fig. 4. We also give examples of failure cases in Fig. 5 to illustrate the highly challenging nature of the confused classes. It is noteworthy to mention that although we run our experiments with a VGGnet model, our proposed spectral features can be used in conjunction with any network configuration.



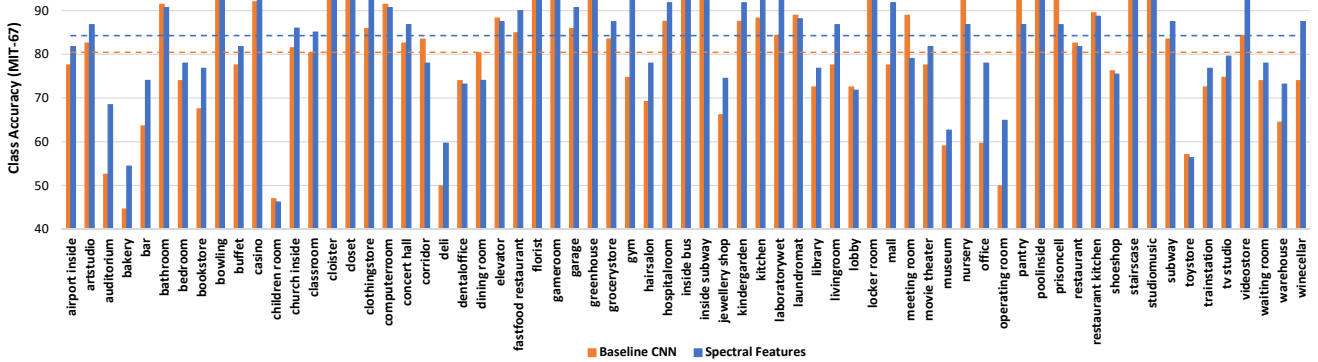


Figure 4: Comparison of class-wise accuracies on the MIT-67 dataset obtained using the baseline and the proposed spectral features based approach. (*Best seen when enlarged*)

Approach	Accuracy (%)
ImageNet-VGGnet-16 [51]	51.7
Hybrid-CNN [67]	53.8
Deep19-DAG CNN [65]	56.2
MetaObject-CNN [63]	58.1
Places-CNDS [60]	60.7
Baseline CNN (Places-VGGnet [59])	66.9
Places-VGGnet + Spectral Features	<b>67.6</b>

Table 3: Average accuracy on the SUN397 Scene Dataset.

#### 4.4. Analysis and Discussion

**Dimensionality Analysis:** We study the relationship between the number of DCT coefficients and the corresponding performance on the MIT-67 dataset (see Fig. 6). An increase in spectral coefficients generally yields an improvement in the classification performance, however beyond the 4096 feature dimension, the trend reaches a plateau and no significant improvement is observed. We notice a slight drop in performance beyond  $\sim 10k$  spectral coefficients. Due to this trend and for the sake of a fair comparison with baseline and VGGnet based approaches that use a 4096-dimensional feature dimension, we use an equidimensional spectral transform in the CNN model.

**Fourier Transform and Phase Information:** We also test the closely related DFT features. For classification purposes, only real-valued feature vectors can be used. Therefore, we analyze the performance independently using the magnitude and phase information as well as the combination of both. For this experiment, we use features before the first FC layer of the VGGnet (pretrained on the Places dataset) and a two-layer MLP classifier for classification after spectral transformation, and feature normalization on the MIT-67 dataset. The results are reported in Table 4. We note that the DFT features perform slightly lower compared to the DCT features, while the phase information performs considerably lower than the magnitude features on the scene classification task. When we concatenate both the normal-

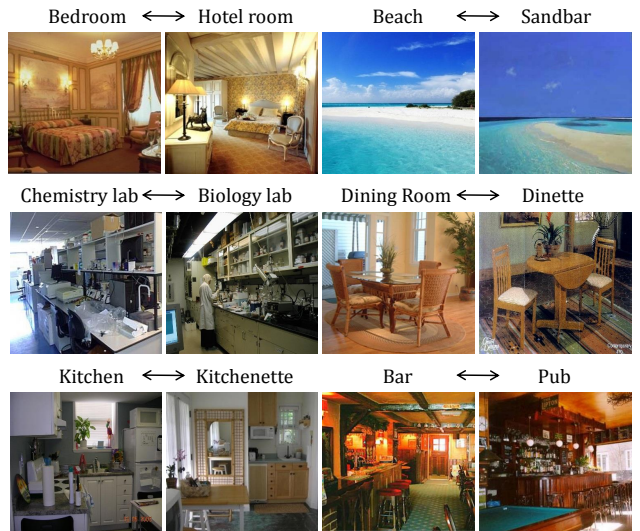


Figure 5: Pairs from the SUN dataset which were confused with each other by the classification algorithm. We also show one example from each class that was mistakenly categorized as the second class.

DCT	DFT Mag.	DFT Phase	DFT Mag. + Phase
80.1	78.2	59.6	74.7

Table 4: Performance comparison between the magnitude and phase components of spectral transform.

ized phase and magnitude feature representations, the resulting accuracy is lower than the performance due to only magnitude features. This indicates that the phase information does not help in scene classification.

**Domain Transfer:** Here, we evaluate the performance of spectral features on the domain transfer task. To this end, we obtained off-the-shelf feature representations before the first fully connected layer of the VGGnet model which is pretrained on the ImageNet objects dataset. Given these features, we apply DCT transform to generate spectral features (10k dimension), which are then used to test the scene clas-

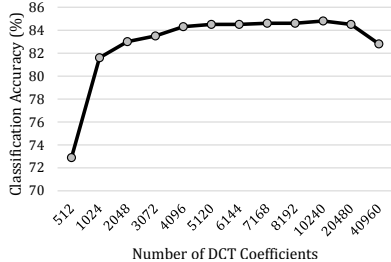


Figure 6: The relationship between the spectral feature dimension and classification accuracy on the MIT-67 dataset.

sification accuracy on a scene-centric dataset (MIT-67). The spectral features were normalized and a linear SVM classifier was used for classification. We notice a significant boost in classification performance compared to normal VGGnet features both with and without data augmentation which depicts the superior discriminative ability of spectral features (see Table 5).

Accuracy (%)	with aug.	w/o aug.
Off-the-shelf feat. + SVM	71.9	64.1
Spectral feat. + SVM	75.7	70.5

Table 5: Improvement due to spectral features when the deep network is trained and tested on different tasks.

**Kernel Transform:** Fourier basis have been used in the previous works to approximate popular kernel transforms [43, 41]. Therefore, one interesting aspect is to compare the classification performance with a Radial Basis Function (RBF) kernel and a DCT transformation. Using features from a VGGnet trained on the Places-205 dataset, we get 79.1% accuracy with a linear SVM and 80.1% with a non-linear SVM using RBF kernel. We noted a similar trend with the features extracted using a VGGnet pretrained on the ImageNet dataset. On the MIT-67 dataset, 71.9% and 73.1% accuracy was achieved using a linear SVM and a nonlinear SVM with RBF kernel, respectively.

**Data Augmentation:** The results reported in § 4.3 use data augmentation for parameter learning and inference. We perform an ablation study to investigate the performance gain with spectral features without any data augmentation on the MIT-67 indoor scene dataset. The results are summarized in Table 6. For the domain adaptation task, where the features from a VGGnet trained on another task are used to classify scenes, we report comparisons with and without data augmentation (see Table 5). Although data augmentation helps in achieving considerably higher performance levels, the additional performance boost due to spectral features is persistent and remarkable even without data augmentation.

**Is Performance Gain due to Increased Depth?** The spectral transformation is implemented as a FC layer in the deep network. This results in an increase in overall depth of the network. One may wonder whether the performance gain is due to the additional depth or the spectral features? To

Accuracy (%)	with aug.	w/o aug.
Places-VGGnet	80.9	77.6
Places-VGGnet (spectral feat)	84.3	81.7

Table 6: The effect of data augmentation on the performance due to spectral features (MIT-67 dataset).

investigate this question, we trained the same network as used for spectral features based classification on the MIT-67 dataset, except that the spectral transform layer is replaced by a normal FC layer with the number of neurons equal to the number of spectral coefficients. This model is considered as the baseline model. Moreover, we also experimented by replacing the DCT transform matrix with a random projection matrix whose columns are mutually independent. The results are summarized in Table 7. We note that an additional FC layer provides an improvement on the MIT-67 dataset, however this improvement is less pronounced compared to the spectral features.

Method	Baseline	Spectral Feat.	Random Proj.
Acc.(%)	81.8	84.3	81.6

Table 7: The comparison between the performance gain due to spectral transformation, learned FC layer and the random projection layer in a deep CNN.

**Feature Decorrelation:** We notice a decrease in feature co-adaptation with the use of spectral transformation. Figure 8 illustrates portions from the data covariance matrix corresponding to the baseline CNN features and the spectral features. The covariance matrix derived from spectral features has a stronger diagonal with much weaker off-diagonal entries compared to the covariance matrix of baseline CNN activations. To quantitatively verify this behavior, we define a diagonalization index ( $\eta$ ) for a matrix  $X \in \mathbb{R}^{n \times n}$  as the ratio:  $\eta = \sum_{i=1}^n X_{i,i} / \sum_{i=1}^n \sum_{j=1}^n X_{i,j}$ . In Table 8, we notice a significant increase in  $\eta$  both for the baseline and spectral features covariance matrices projected onto the DCT basis function (defined in Eq. 4). The  $\eta$  index of 1 is the ideal case, where the unitary transformation  $Q_n$  is composed of eigenvectors of the data covariance matrix.

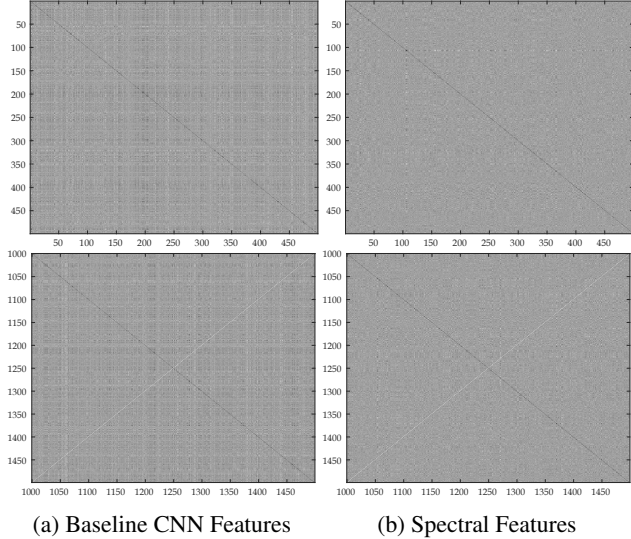
Matrix	$C_{b-cnn}$	$A_{b-cnn}$	$C_{spec-cnn}$	$A_{opt}$
$\eta$ index	0.002	0.721	0.820	1.0

Table 8: The diagonalization measure for different covariance and projected matrices.

**Generalization:** To study the generalization of spectral transformation to other architectures, we tested with GoogleNet and ResNet models pre-trained on the Places-205 dataset. While evaluated on MIT67 dataset, the proposed method achieves a classification accuracy of 77.3%



Figure 7: **Left** box shows sample attribute predictions for the Outdoor Scene Attribute dataset. **Right** box shows sample results on the SUN Attribute dataset, which contains more fine-grained and localized attributes.



(a) Baseline CNN Features (b) Spectral Features  
Figure 8: Portions of covariance matrices corresponding to baseline CNN features and spectral features. Feature detectors after spectral transformation are significantly decorrelated. See Table 8 for the diagonalization index ( $\eta$ ) values.

compared with 75.1% using GoogleNet and 79.1% compared with 76.8% using ResNet model.

We also tested on the related task of object classification using Caltech-101 dataset. Using the baseline CNN with initial layers pre-trained on the ImageNet dataset and final layers on the object dataset, we obtained an accuracy of 90.5%. With the proposed spectral transformation layer and keeping other hyper-parameters same, the accuracy increased to 91.7%.

## 5. Scene Attribute Detection

In this section, we are interested in investigating the relationship between spectral features and visual attributes. The scene attributes are semantically meaningful mid-level representations which are not only used by humans for scene description, but have also been found very useful for tasks such as caption generation, image retrieval and zero-shot learning [44]. Specifically, we experiment on two publicly available scene attribute datasets:

**SUN Attribute Dataset** [39] consists of 14,000 scene im-

Method	SUN-Att	SceneAtt
cKernel+SVM [39]	87.9	64.5
HST-att [61]	-	67.6
Spec Feat + SVM	<b>90.3</b>	<b>94.6</b>

Table 9: Classification performance in terms of mean Average Precision (mAP).

ages labeled with 102 distinct attributes. The attributes relate to functional characteristics, materials, surface properties and the global spatial envelope.

**Outdoor Scene Attribute Dataset** [61] contains 1226 scene images with 31 attributes as noun-adjective pairs.

**Results:** For both the datasets, we follow standard protocols as described in [39, 61]. The proposed spectral features are obtained from the pretrained Paces-VGG network and binary SVM classifiers are trained for each attribute. Qualitative attribute predictions are shown in Fig. 7. Note that the SUN attribute dataset contain attribute labeling for actions and scenarios which may not be present in the scene but *may occur* depending on the scene type. Quantitative results are summarized in Table 9. There is a relatively less pronounced increase in attribute recognition performance on the SUN Attribute dataset. One possible reason can be that most of the attributes relate to more fine-grained and region specific local information, while the proposed descriptor works on global level in our experiments.

## 6. Conclusion

This paper presents a spectral domain feature representation on top of the convolution activations from a deep network. The spectral transformation enhances the discriminative ability of deep network by decorrelating the individual feature detectors, thus introducing a regularization effect. Our implementation does not introduce any significant computational cost. We tested our approach on three large-scale scene-centric datasets and reported encouraging improvements on the baseline CNN features. We also performed a detailed ablative analysis to validate the performance improvement. Finally, our experiments on attribute detection using spectral features demonstrated their superior ability to encode semantic cues relating to indoor and outdoor scenes.



## References

- [1] N. Ahmed and K. R. Rao. *Orthogonal transforms for digital signal processing*. Springer Science & Business Media, 2012.
- [2] S. An, M. Hayat, S. H. Khan, M. Bennamoun, F. Boussaid, and F. Sohel. Contractive rectifier networks for nonlinear maximum margin classification. In *Proceedings of the IEEE international conference on computer vision*, pages 2515–2523, 2015.
- [3] A. Babenko, A. Slesarev, A. Chigorin, and V. Lempitsky. Neural codes for image retrieval. In *European Conference on Computer Vision*, pages 584–599. Springer, 2014.
- [4] S. Ben-Yacoub, B. Fasel, and J. Luetin. Fast face detection using mlp and fft. In *Proc. Second International Conference on Audio and Video-based Biometric Person Authentication (AVBPA' 99)*, number EPFL-CONF-82563, pages 31–36, 1999.
- [5] I. Biederman. Recognition-by-components: a theory of human image understanding. *Psychological review*, 94(2):115, 1987.
- [6] A. Bosch, A. Zisserman, and X. Muoz. Scene classification using a hybrid generative/discriminative approach. *Transactions on Pattern Analysis and Machine Intelligence*, 30(4):712–727, 2008.
- [7] A. Böttcher and S. M. Grudsky. *Toeplitz matrices, asymptotic linear algebra, and functional analysis*. Birkhäuser, 2012.
- [8] L. Breiman. Bagging predictors. *Machine learning*, 24(2):123–140, 1996.
- [9] J. Bruna and S. Mallat. Invariant scattering convolution networks. *IEEE transactions on pattern analysis and machine intelligence*, 35(8):1872–1886, 2013.
- [10] W. Chen, J. T. Wilson, S. Tyree, K. Q. Weinberger, and Y. Chen. Compressing convolutional neural networks. *arXiv preprint arXiv:1506.04449*, 2015.
- [11] Y. Cheng, F. X. Yu, R. S. Feris, S. Kumar, A. Choudhary, and S.-F. Chang. An exploration of parameter redundancy in deep networks with circulant projections. In *Proceedings of the IEEE International Conference on Computer Vision*, pages 2857–2865, 2015.
- [12] B. Cheung, J. A. Livezey, A. K. Bansal, and B. A. Olshausen. Discovering hidden factors of variation in deep networks. *arXiv preprint arXiv:1412.6583*, 2014.
- [13] M. Cimpoi, S. Maji, I. Kokkinos, and A. Vedaldi. Deep filter banks for texture recognition, description, and segmentation. *International Journal of Computer Vision*, 118(1):65–94, 2016.
- [14] M. Cogswell, F. Ahmed, R. Girshick, L. Zitnick, and D. Batra. Reducing overfitting in deep networks by decorrelating representations. *arXiv preprint arXiv:1511.06068*, 2015.
- [15] C. Doersch, A. Gupta, and A. A. Efros. Mid-level visual element discovery as discriminative mode seeking. In *Advances in Neural Information Processing Systems*, pages 494–502, 2013.
- [16] M. George, M. Dixit, G. Zogg, and N. Vasconcelos. Semantic clustering for robust fine-grained scene recognition. In *European Conference on Computer Vision*, pages 783–798. Springer, 2016.
- [17] Y. Gong, L. Wang, R. Guo, and S. Lazebnik. Multi-scale orderless pooling of deep convolutional activation features. In *European Conference on Computer Vision*, pages 392–407. Springer, 2014.
- [18] R. M. Gray et al. Toeplitz and circulant matrices: A review. *Foundations and Trends® in Communications and Information Theory*, 2(3):155–239, 2006.
- [19] U. Grenander and G. Szegö. *Toeplitz forms and their applications*, volume 321. Univ of California Press, 2001.
- [20] M. Hayat, S. H. Khan, M. Bennamoun, and S. An. A spatial layout and scale invariant feature representation for indoor scene classification. *IEEE Transactions on Image Processing*, 25(10):4829–4841, Oct 2016.
- [21] M. Hayat, S. H. Khan, N. Werghi, and R. Goecke. Joint registration and representation learning for unconstrained face identification. In *Proceedings of the IEEE Conference on Computer Vision and Pattern Recognition*, pages –, 2017.
- [22] K. He, X. Zhang, S. Ren, and J. Sun. Spatial pyramid pooling in deep convolutional networks for visual recognition. In *European Conference on Computer Vision*, pages 346–361. Springer, 2014.
- [23] K. He, X. Zhang, S. Ren, and J. Sun. Deep residual learning for image recognition. *arXiv preprint arXiv:1512.03385*, 2015.
- [24] A. J. Hoffman, H. W. Wielandt, et al. The variation of the spectrum of a normal matrix.
- [25] S. Ioffe and C. Szegedy. Batch normalization: Accelerating deep network training by reducing internal covariate shift. In *Proceedings of the 32nd International Conference on Machine Learning (ICML-15)*, pages 448–456, 2015.
- [26] K. Jarrett, K. Kavukcuoglu, Y. Lecun, et al. What is the best multi-stage architecture for object recognition? In *2009 IEEE 12th International Conference on Computer Vision*, pages 2146–2153. IEEE, 2009.
- [27] M. Juneja, A. Vedaldi, C. Jawahar, and A. Zisserman. Blocks that shout: Distinctive parts for scene classification. In *International Conference on Computer Vision and Pattern Recognition*, pages 923–930. IEEE, 2013.
- [28] S. H. Khan, M. Bennamoun, F. Sohel, and R. Togneri. Cost sensitive learning of deep feature representations from imbalanced data. *IEEE transactions on neural networks and learning systems*, 2017.
- [29] S. H. Khan, M. Hayat, M. Bennamoun, R. Togneri, and F. A. Sohel. A discriminative representation of convolutional features for indoor scene recognition. *IEEE Transactions on Image Processing*, 25(7):3372–3383, 2016.
- [30] S. H. Khan, X. He, F. Porikli, M. Bennamoun, F. Sohel, and R. Togneri. Learning deep structured network for weakly supervised change detection. *Proceedings of the International Joint Conference on Artificial Intelligence*, 2017.
- [31] A. Krizhevsky, I. Sutskever, and G. E. Hinton. Imagenet classification with deep convolutional neural networks. In *Advances in Neural Information Processing Systems*, pages 1097–1105, 2012.
- [32] A. Lavin. Fast algorithms for convolutional neural networks. *arXiv preprint arXiv:1509.09308*, 2015.

- [33] S. Lazebnik, C. Schmid, and J. Ponce. Beyond bags of features: Spatial pyramid matching for recognizing natural scene categories. In *International Conference on Computer Vision and Pattern Recognition*, volume 2, pages 2169–2178. IEEE, 2006.
- [34] J. Long, E. Shelhamer, and T. Darrell. Fully convolutional networks for semantic segmentation. In *Proceedings of the IEEE Conference on Computer Vision and Pattern Recognition*, pages 3431–3440, 2015.
- [35] M. Mathieu, M. Henaff, and Y. LeCun. Fast training of convolutional networks through ffts. *arXiv preprint arXiv:1312.5851*, 2013.
- [36] A. Oliva and A. Torralba. Modeling the shape of the scene: A holistic representation of the spatial envelope. *International Journal of Computer Vision*, 42(3):145–175, 2001.
- [37] A. Oliva, A. Torralba, A. Guérin-Dugué, and J. Hérault. Global semantic classification of scenes using power spectrum templates. In *Proceedings of the 1999 international conference on Challenge of Image Retrieval*, pages 9–9. British Computer Society, 1999.
- [38] A. V. Oppenheim and R. W. Schaffer. *Discrete-time signal processing*. Pearson Higher Education, 2010.
- [39] G. Patterson, C. Xu, H. Su, and J. Hays. The sun attribute database: Beyond categories for deeper scene understanding. *International Journal of Computer Vision*, 108(1-2):59–81, 2014.
- [40] N. Pinto, D. Doukhan, J. J. DiCarlo, and D. D. Cox. A high-throughput screening approach to discovering good forms of biologically inspired visual representation. *PLoS Comput Biol*, 5(11):e1000579, 2009.
- [41] F. Porikli and H. Ozkan. Data driven frequency mapping for computationally scalable object detection. In *IEEE Advanced Video and Signal based Surveillance (AVSS)*, 2011.
- [42] A. Quattoni and A. Torralba. Recognizing indoor scenes. In *International Conference on Computer Vision and Pattern Recognition*. IEEE, 2009.
- [43] A. Rahimi and B. Recht. Random features for large-scale kernel machines. In *Advances in neural information processing systems*, pages 1177–1184, 2007.
- [44] S. Rahman, S. H. Khan, and F. Porikli. A unified approach for conventional zero-shot, generalized zero-shot and few-shot learning. *arXiv preprint arXiv:1706.08653*, 2017.
- [45] K. R. Rao and P. Yip. *Discrete cosine transform: algorithms, advantages, applications*. Academic press, 2014.
- [46] A. S. Razavian, H. Azizpour, J. Sullivan, and S. Carlsson. Cnn features off-the-shelf: an astounding baseline for recognition. *arXiv preprint arXiv:1403.6382*, 2014.
- [47] S. Ren, K. He, R. Girshick, and J. Sun. Faster r-cnn: Towards real-time object detection with region proposal networks. In *Advances in neural information processing systems*, pages 91–99, 2015.
- [48] O. Rippel, J. Snoek, and R. P. Adams. Spectral representations for convolutional neural networks. In C. Cortes, N. D. Lawrence, D. D. Lee, M. Sugiyama, and R. Garnett, editors, *Advances in Neural Information Processing Systems 28*, pages 2440–2448. Curran Associates, Inc., 2015.
- [49] A. Saxe, P. W. Koh, Z. Chen, M. Bhand, B. Suresh, and A. Y. Ng. On random weights and unsupervised feature learning. In *Proceedings of the 28th international conference on machine learning (ICML-11)*, pages 1089–1096, 2011.
- [50] A. Sharif Razavian, H. Azizpour, J. Sullivan, and S. Carlsson. Cnn features off-the-shelf: an astounding baseline for recognition. In *Proceedings of the IEEE Conference on Computer Vision and Pattern Recognition Workshops*, pages 806–813, 2014.
- [51] K. Simonyan and A. Zisserman. Very deep convolutional networks for large-scale image recognition. *CoRR*, abs/1409.1556, 2014.
- [52] N. Srivastava, G. E. Hinton, A. Krizhevsky, I. Sutskever, and R. Salakhutdinov. Dropout: a simple way to prevent neural networks from overfitting. *Journal of Machine Learning Research*, 15(1):1929–1958, 2014.
- [53] C. Szegedy, W. Liu, Y. Jia, P. Sermanet, S. Reed, D. Anguelov, D. Erhan, V. Vanhoucke, and A. Rabinovich. Going deeper with convolutions. In *Proceedings of the IEEE Conference on Computer Vision and Pattern Recognition*, pages 1–9, 2015.
- [54] A. Torralba and A. Oliva. Statistics of natural image categories. *Network: computation in neural systems*, 14(3):391–412, 2003.
- [55] S. K. Ungerleider and L. G. Mechanisms of visual attention in the human cortex. *Annual review of neuroscience*, 23(1):315–341, 2000.
- [56] N. Vasilache, J. Johnson, M. Mathieu, S. Chintala, S. Piantino, and Y. LeCun. Fast convolutional nets with fbfft: A gpu performance evaluation. *arXiv preprint arXiv:1412.7580*, 2014.
- [57] W. E. Vinje and J. L. Gallant. Sparse coding and decorrelation in primary visual cortex during natural vision. *Science*, 287(5456):1273–1276, 2000.
- [58] L. Wan, M. Zeiler, S. Zhang, Y. L. Cun, and R. Fergus. Regularization of neural networks using dropconnect. In *Proceedings of the 30th International Conference on Machine Learning (ICML-13)*, pages 1058–1066, 2013.
- [59] L. Wang, S. Guo, W. Huang, and Y. Qiao. Places205-vggnet models for scene recognition. *arXiv preprint arXiv:1508.01667*, 2015.
- [60] L. Wang, C.-Y. Lee, Z. Tu, and S. Lazebnik. Training deeper convolutional networks with deep supervision. *arXiv preprint arXiv:1505.02496*, 2015.
- [61] S. Wang, J. Joo, Y. Wang, and S.-C. Zhu. Weakly supervised learning for attribute localization in outdoor scenes. In *Proceedings of the IEEE Conference on Computer Vision and Pattern Recognition*, pages 3111–3118, 2013.
- [62] J. Wu and J. M. Rehg. Centrist: A visual descriptor for scene categorization. *Transactions on Pattern Analysis and Machine Intelligence*, 33(8):1489–1501, 2011.
- [63] R. Wu, B. Wang, W. Wang, and Y. Yu. Harvesting discriminative meta objects with deep cnn features for scene classification. In *Proceedings of the IEEE International Conference on Computer Vision*, pages 1287–1295, 2015.
- [64] J. Xiao, J. Hays, K. A. Ehinger, A. Oliva, and A. Torralba. Sun database: Large-scale scene recognition from abbey to

- zoo. In *International Conference on Computer Vision and Pattern Recognition*, pages 3485–3492. IEEE, 2010.
- [65] S. Yang and D. Ramanan. Multi-scale recognition with dag-cnns. In *Proceedings of the IEEE International Conference on Computer Vision*, pages 1215–1223, 2015.
- [66] B. Zhou, A. Khosla, A. Lapedriza, A. Oliva, and A. Torralba. Object detectors emerge in deep scene cnns. *arXiv preprint arXiv:1412.6856*, 2014.
- [67] B. Zhou, A. Lapedriza, J. Xiao, A. Torralba, and A. Oliva. Learning deep features for scene recognition using places database. In *Advances in neural information processing systems*, pages 487–495, 2014.
- [68] H. Zhou, J. Alvez, and F. Porikli. Less is more: Towards compact cnns,. In *Proceedings of the European Conference on Computer Vision*, 2016.